

Planetary Radar Imaging with the Deep-Space Network’s 34 meter Uplink Array

V. Vilnrotter¹, P. Tsao, D. Lee, T. Cornish, J. Jao, M. Slade
Jet Propulsion Laboratory, California Institute of Technology
4800 Oak Grove Drive
Pasadena, CA, 91109
(818) 354-2745
Victor.A.Vilnrotter@jpl.nasa.gov

Abstract— A coherent uplink array consisting of up to three 34-meter antennas of NASA’s Deep Space Network has been developed for the primary purpose of increasing EIRP at the spacecraft. Greater EIRP ensures greater reach, higher uplink data rates for command and configuration control, as well as improved search and recovery capabilities during spacecraft emergencies. It has been conjectured that Doppler-delay radar imaging of lunar targets can be extended to planetary imaging, where the long baseline of the uplink array can provide greater resolution than a single antenna, as well as potentially higher EIRP. However, due to the well known R^4 loss in radar links, imaging of distant planets is a very challenging endeavor, requiring accurate phasing of the Uplink Array antennas, cryogenically cooled low-noise receiver amplifiers, and sophisticated processing of the received data to extract the weak echoes characteristic of planetary radar. This article describes experiments currently under way to image the planets Mercury and Venus, highlights improvements in equipment and techniques, and presents planetary images obtained to date with two 34 meter antennas configured as a coherently phased Uplink Array.

is in the far-field of compact arrays of 34 meter antennas, such as the Apollo cluster of three 34 meter antennas at Goldstone, spanning half a kilometer. These antennas are designated as “Deep-Space Station 24/25/26”, or DSS-24/25/26. Far-field calibration enables the direct measurement of combined array power in a given direction, thus providing direct verification of Uplink Array calibration through power maximization over the desired target as described in [1].

Uplink array calibration requires electronic fine-tuning of the array beam to point precisely in the desired direction, which can be accomplished by imaging a well-known target in the far-field of the array. The central peak of the lunar crater Tycho was selected as the radar target, due to its well-known ephemeris and visibility every day of the year. During calibration the uplink array is pointed towards Tycho, a known pseudonoise modulated X-band signal is transmitted simultaneously from two or three 34 meter antennas, and the echo received by another 34 meter antenna where it is processed to obtain a Doppler-delay image of the far-field array illumination. Finally, the brightest array fringe is centered over the target via phase adjustments on the ground.

The signal power reflected from the Moon and planets, as well as Doppler-spread and delay-dispersion characteristics can be estimated from a simplified model that assigns beamwidths to the array antennas, and assumes a simple scattering model for the lunar and planetary surfaces. Although the Moon nominally presents the same face to the Earth at all times, it actually exhibits a small apparent spin called libration, the largest component of which is earth-rotation, called diurnal libration (the other components are longitude and latitude libration). The maximum apparent spin rate of the Moon due to diurnal libration is approximately $\omega = 1.2 \times 10^{-6}$ rad/sec at the Earth’s equator, therefore the approaching and receding limbs at the lunar equator impart approximately 1.2×10^{-6} rad/sec at transit [2]. It follows that approaching and receding limbs at the lunar equator move towards or away from the Earth at approximately $v = \pm R_{Moon} \omega = (1.75 \times 10^6)(1.2 \times 10^{-6}) \cong 2$ m/s. At the standard DSN uplink carrier frequency of roughly 7.15 GHz this apparent lunar rotation produces

TABLE OF CONTENTS

1. INTRODUCTION.....	1
2. EXPECTED SNR AND DOPPLER FOR MOON-BOUNCE CALIBRATION.....	1
3. MATHEMATICAL MODEL AND SIGNAL PROCESSING ALGORITHM.....	4
4. EXPERIMENTAL RESULTS.....	5
5. SUMMARY AND CONCLUSIONS.....	12
REFERENCES.....	12
BIOGRAPHY.....	12

1. INTRODUCTION

Doppler-delay imaging of small, high-reflectivity radar targets on the Moon is an emerging technology capable of calibrating Uplink Arrays currently under consideration for future Deep Space Network (DSN) applications. The Moon

¹ Authors are with the Jet Propulsion Laboratory, California Institute of Technology.

Doppler frequencies of approximately $f_D = \pm f(v/c) = \pm(7.15 \times 10^9)(2/3)10^{-8} \cong \pm 50$ Hz, hence we shall assume a limb-to-limb Doppler spread of 100 Hz in the following calculations.

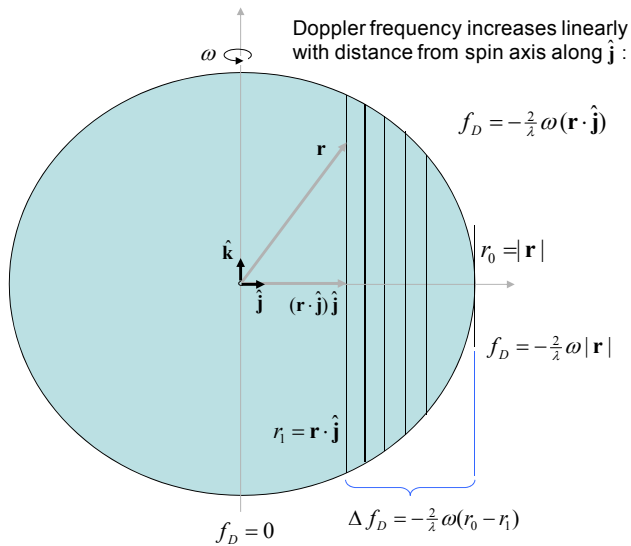


Figure 1a). Geometrical construction showing that frequency increases linearly from center, generating constant frequency “Doppler slices” parallel to the apparent spin axis.

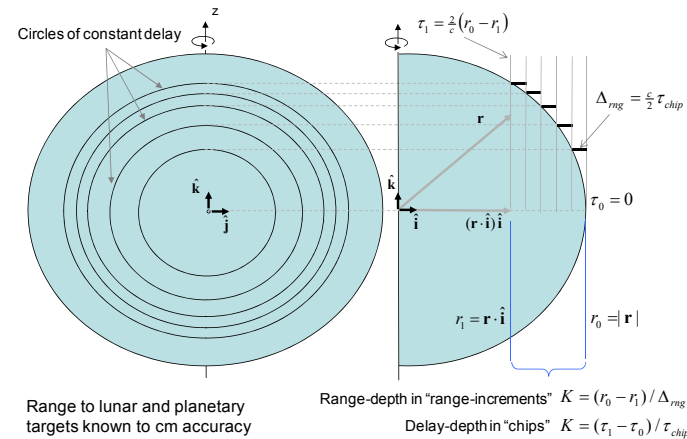


Figure 1b). Geometrical construction showing circles of constant delay, with definition of “range-increments” and “delay-depth”.

The geometrical construction shown in Fig. 1 a) demonstrates that Doppler is distributed uniformly across the apparent lunar equator, forming in effect “slices” of constant Doppler parallel to the spin axis: since the lunar diameter is approximately 3500 km, the change in frequency perpendicular to the spin-axis is roughly $100/3500 \cong 0.03$ Hz/km.

The mean surface is approximately spherical, which means that the signal reflected from the closest point (apparent center, or “sub-radar point”) has the least delay, with increasing delay along concentric rings of greater radius. As

shown in Fig. 1b, signals reflected by features some distance from the apparent lunar center travel the extra distance twice, hence the delay spread of the Moon can be expressed as $\delta = 2R_{Moon}/c = 3.5 \times 10^6 / 3 \times 10^8 \cong 12$ ms.

The expected Doppler-spread due to relative planetary orbital dynamics can be estimated in a similar manner, by first determining planetary spin, then calculating the resulting Doppler as seen from the earth. Estimation of the Doppler spread of a planet or asteroid requires knowledge of the motion of the subradar point in planetographic (selenographic for the Moon) coordinates $\theta(t)$.

$$\Delta v = 2r \frac{d\theta(t)}{dt}$$

where r is the radius. The tables for this information are contained in [7]. The pointing-based predicts that are generated using NAIF SPICE take into account the finite speed of light and the effect of stellar aberration. Stellar aberration is an apparent motion induced by motion of the observer or target that is transverse to incoming or outgoing radiation [8]. The predicts from the Goldstone Solar System Radar (GSSR) group also consider the increase in optical path length from gravitational lensing by massive Solar System objects [9].

Highly reflective features on the Moon such as the center of the crater Tycho, provide a convenient target for uplink array calibration, henceforth termed “Moon-Bounce Calibration” in the rest of this paper. The lunar surface imparts different Doppler to radio signals reflected from thin “slices” parallel to the apparent spin axis of the Moon. As shown in Fig. 1 b), the near-spherical mean surface can be viewed as a sequence of concentric rings of increasing radius, corresponding to increasing delay in the echo as observed by the receiver. The intersection of Doppler slices and concentric delay rings give rise to pixels on the lunar surface with distinct Doppler-delay signatures, which can be used to isolate specific features on the lunar surface.

2. EXPECTED SNR AND DOPPLER FOR MOON-BOUNCE AND PLANETARY IMAGING

As an example of the achievable SNR for lunar and planetary imaging with the Uplink Array, consider an array of two $d = 34$ m beam-waveguide (BWG) yields a maximal primary beam of approximately $\lambda d = 0.04/34 = 1.2$ mrad where λ is wavelength, equal to 4 cm at 7.15 GHz, and a minimal array beamwidth of λ/D mrad, where D is the distance between the two antennas, forming an array beam with peaks and nulls perpendicular to the baseline. With this model, the transmitted power is contained uniformly within a cone of apex angle of λ/d and circular base of area $A_t = 4\pi (\lambda R/d_t)^2$ at a distance R from the transmitter. If

each 34 m antenna transmits $P_t = 20 \text{ kW}$, the power density at a distance R from a single antenna is $P_t / A_t \cong 2 \times 10^{10} / R^2 \text{ W/m}^2$, but actually a factor of 4 greater over peaks of constructive interference. If the radar target is greater than footprint of the beam, A_t , then all of the transmitted power is captured, and a fraction σ_r reflected back toward the transmitter, where σ_r is called the “reflection coefficient” and is typically approximately 0.01-0.1 for lunar and planetary targets.

If the radar target is smaller than A_t , then only a fraction $\sigma_r \delta_r = \sigma_r a_t / A_t$ is reflected, where a_t is the effective radar cross-section of the target, generally smaller than the apparent physical area, and $\delta_r = \min(1, a_t / A_t)$. It is assumed that the radar target scatters the reflected power into a cone of 1 radian apex angle, somewhat like a Lambertian reflector, generating a footprint of approximate diameter R at a distance R : therefore, a receiving antenna near the transmitter with diameter d_r collects a fraction $(d_r / R)^2$ of the total reflected power. In addition, effective antenna efficiencies at X-band are typically 70%, hence we include another factor $\eta_{rt} = (0.7)^2 = 0.5$ to account for realistic losses within the transmitting and receiving antennas.

With the above model, the echo power collected by a receiving antenna with diameter d_r , scattered from a radar target at a distance R illuminated by a transmitting antenna with diameter d_t , is of the form:

$$P_r = \delta_r \sigma_r \eta_{rt} P_t \left(\frac{d_r}{2R} \right)^2 = \delta_r \sigma_r \eta_{rt} P_t \left(\frac{d_r}{R} \right)^2 \quad (1)$$

Note that if the target area is greater than the footprint of the transmitted beam, then this equation exhibits an R^{-2} dependence of the received radar power. Otherwise, the R^2 dependence of A_t also comes into effect, yielding a combined R^{-4} dependence of received power on range, when the area of the target is smaller than the signal footprint.

The noise power at the output of a receiver with bandwidth B and effective system temperature of T_{sys} kelvins, which includes contributions from the receiver electronics as well as external sources such as the cosmic background (3 kelvins) and the troposphere (which is elevation dependent, with approximately 10 kelvins at zenith), and given by $P_n = k T_{\text{sys}} B$, where $k = 1.38 \times 10^{-23} \text{ joules/kelvin}$ is Boltzmann’s constant.

The signal-to-noise power ratio, $SNR = P_r / P_n$, provides an indication of the “detectability” of the radar echo, and a useful check on experimentally measured power levels. Taking the ratio of received Doppler-spread scattered signal power to receiver noise power in the Doppler-spread bandwidth B , yields:

$$SNR = \frac{P_r}{P_n} = \frac{\delta_r \sigma_r \eta_{rt} P_t}{k T_{\text{sys}} B} \left(\frac{d_r^2}{R^2} \right) \quad (2)$$

Next, we apply equation (2) to examples of Doppler-delay imaging of the Moon, Mercury and Venus.

a) SNR for Lunar Doppler-delay Imaging.

The Tycho region of the Moon was imaged most frequently in the past as part of the Uplink Array calibration effort, as described in [1, 2]. The Tycho region is in the lunar southern hemisphere, inclined at an angle of approximately 45 degrees to the incident illumination. We assume a scattered reflection coefficient in this inclined region of approximately $\sigma_r = 0.01$, meaning that only one hundredth of the incident power is reflected back towards the transmitter, and further assume that the system temperature of the room-temperature receiver is $T_{\text{sys}} = 100$ kelvins.

Letting $R = 4 \times 10^8 \text{ m}$, $d_r = 34 \text{ m}$, $P_t = 2 \times 10^4 \text{ W}$,

$\lambda = 0.04 \text{ m}$, $\delta_r = 1$ and $B = 100 \text{ Hz}$, equation (2) yields:

$$SNR = \frac{0.01 \times 0.5 (2 \times 10^4) (1.156 \times 10^3)}{100 (1.38 \times 10^{-23}) (1.6 \times 10^{19}) 100} = \frac{1.16 \times 10^5}{2.21 \times 10^{-2}} \cong 5 \times 10^6$$

or about 67 dB. This rough value is consistent with the measured spectral density shown in Fig. 4 a), where the spectral level continues to decrease outside the range shown in the graph to below -60 dB.

b) SNR Calculations for Mercury Doppler-delay Imaging

Although somewhat larger than the Moon, Mercury is so much further even at closest approach that it subtends a much smaller angular diameter, or equivalently, its effective radar cross-section is so much smaller that it intercepts only a tiny fraction of the transmitted power. At the encounter distance of $R = 0.56 \text{ AU} = 84 \text{ million kilometers}$, the 4880 km diameter of Mercury’s disk subtends only an angle of 0.06 mrad, with an effective radar cross-section of roughly half that, or 0.03 mrad, and a Doppler-spread of 300 Hz. Since most of the reflections arise from the sub-radar point implying normal incidence and reflection, the scattering coefficient is set to $\sigma_r = 0.1$, and the attenuation coefficient set to $\delta_r = a_r / A_t = (0.03)^2 = 9 \times 10^{-4}$.

For the Mercury encounter a cryogenic LNA front-end was used, with an effective system temperature of $T_{\text{sys}} = 36$ kelvins, and the transmitter power was again 20 kW. Substituting into equation (2) yields:

$$\text{SNR} = \frac{\delta_r \sigma_r \eta_r P_t \left(\frac{d_r^2}{R^2} \right)}{k T_{\text{sys}} B} = \frac{0.1 \times 0.5 (9 \times 10^{-4}) (2 \times 10^4) (1.156 \times 10^3)}{36 (1.38 \times 10^{-23}) (300) (7.06 \times 10^{21})}$$

$$= \frac{1.05 \times 10^3}{1.04 \times 10^3} \cong 1$$

or about 0 dB. As shown in Fig. 11a) the value observed on DOY-121 was somewhat lower, but not significantly so.

c) SNR Calculations for Venus Doppler-delay imaging.

The SNR calculations for Venus and Mercury are similar, with the exception that Venus has a thick atmosphere which attenuates both the X-band illumination and reflection, resulting in about 10 dB (factor of ten) additional loss. With a diameter of 12100 km Venus is much larger than Mercury, but on October 24th (DOY-297) at a distance of 0.275 AU or 41 million km still only subtends an angle of 0.3 mrad, or an effective radar cross-section of 0.15 mrad, yielding a fill-factor loss of $\delta_r = 2.25 \times 10^{-2}$. Accounting for the additional loss through the atmosphere of a factor of 0.25, and with a Doppler-spread of 100 Hz, the SNR from Venus on Doy-297 is estimated to be

$$\text{SNR} = \frac{\delta_r \sigma_r \eta_r P_t \left(\frac{d_r^2}{R^2} \right)}{k T_{\text{sys}} B} = \frac{0.1 \times 0.1 \times 0.5 (2.25 \times 10^{-2}) (2 \times 10^4) (1.156 \times 10^3)}{36 (1.38 \times 10^{-23}) (100) (1.7 \times 10^{21})}$$

$$= \frac{2.6 \times 10^3}{8.4 \times 10^1} \cong 30.8$$

or about 14.9 dB. This is comparable to the received SNR observed in real-time with the RSR as shown in Figs. 13 and 14, when Venus was illuminated with a single antenna.

3. UPLINK ARRAY FREQUENCY AND RANGE PREDICTS

The requirement to maintain coherence of uplink array carriers at the target planet (or spacecraft) made it necessary to refine the existing single-antenna frequency and range predicts, and in effect develop a new approach to generate greatly improved differential frequency predicts specifically for Uplink Arraying applications [3]. With the relatively long baselines formed by the Apollo complex (258m to 500m), it was found necessary to refine the positions of the antenna phase centers. The long baselines lead directly to time-varying differential Doppler between the array antennas (due primarily to earth-rotation), hence any inaccuracy in the antenna position vectors can lead to significant frequency prediction errors.

The pointing-vector approach to frequency predicts is based on the observation that differential Doppler frequencies are the most important components of the frequency predicts for array applications, instead of absolute frequency accuracy. In general, frequency predicts are designed to freeze the received frequency at the spacecraft at a predetermined value, by cancelling Doppler due to earth rotation and spacecraft trajectory dynamics. However, the Small Deep-Space Transponder (SDST) aboard EPOXI operates with a 100 Hz loop bandwidth, and therefore it can easily track out small deviations from the design frequency after signal acquisition: therefore, it is sufficient to relate the frequency predicts for the array antennas to the reference antenna predicts, which need to be accurate enough to enable tracking by the SDST.

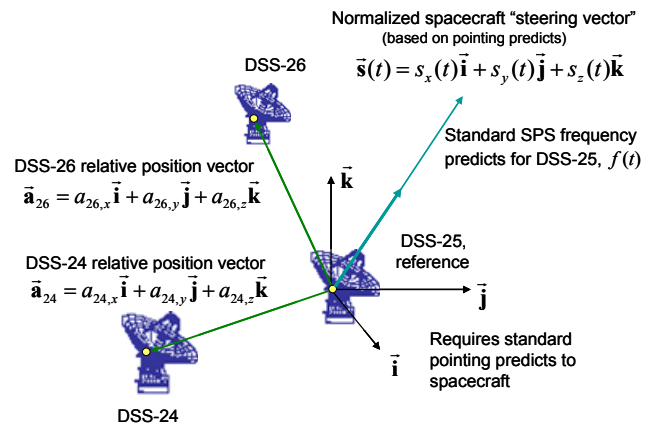


Figure 2. Apollo station antenna geometry, illustrating the relative-frequency predict generation technique developed for uplink arraying.

Referring to Fig. 2, the position vectors from the reference antenna, DSS-25, to the array antennas (DSS-24/26) have been determined to millimeter accuracy, using very accurate VLBI derived solutions. These position vectors refer to the phase-centers of the antennas, which are defined as the intersection of the azimuth and elevation axes. The antennas must be pointed towards the spacecraft to within a small fraction of their 70 millidegree beamwidths, however this is accomplished routinely using operational pointing predicts derived from earth and spacecraft ephemerides. Using any adequate single-antenna frequency predict for DSS-25 as reference, the differential frequencies for the auxiliary array antennas can be obtained by forming the inner product of the normalized pointing vector and the position vector from the reference antenna, as shown in Fig. 2, for each predict-point in time.

The pointing based frequency predicts were originally optimized for Uplink Array Moon-Bounce experiments. For radar imaging of terrestrial planets, some simplifying approximations were introduced and the resulting error sources were believed to be too small to warrant further consideration. For Moon-Bounce experiments, the target

was usually a specific point on the surface of the moon (center of Tycho or Eudoxus) for which a solution was easily obtainable from the NAIF SPICE toolkit. For terrestrial planets, the target was the sub-radar point, the dynamic position of which on the planet surface is less trivial to calculate. As a result, frequency predicts were computed assuming the target was the planet barycenter (easily obtainable from NAIF SPICE). This approximation is reasonable since the relative velocity of the sub-radar point is nearly identical to the relative velocity of the target planet barycenter, when perfectly smooth planetary surfaces are assumed.

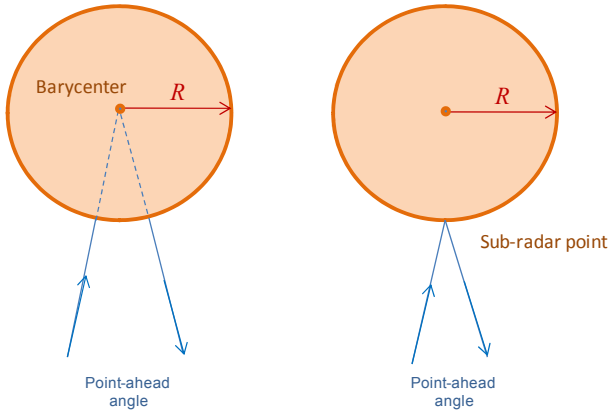


Figure 3. Definition of barycenter and sub-radar point used for planetary range calculations.

As shown in Fig. 3, the difference in two-way range is more substantial and is slightly more than twice the mean radius of the target body. For the purpose of range compensation, twice the mean radius is subtracted leaving a small residual error that is disregarded since it is the *range rate* (relative velocity) that is important for range compensation.

Errors in the relative velocity would result in smearing in range and Doppler of the delay-doppler data. In the case of the Uplink Array, as long as the same approximations are consistently applied for all transmitting stations, the outcome would be the same as the case of a single uplink station.

4. EXPERIMENTAL RESULTS

This section presents experimental results for Doppler-delay imaging of the crater Tycho, the planet Mercury, and the planet Venus. The Uplink Array Doppler-delay imaging concept described in [1, 2, 3] was implemented and tested at the Goldstone Deep Space Communications Complex (GDSCC) near Fort Irwin, California. Three identical 34-m BWG antennas at the Apollo Complex were used to form two- and three-element arrays for the field experiments. Each antenna was equipped with a 20-kW transmitter and was driven by nominally 7.15-GHz signals generated at

Signal Processing Center (SPC) 10, located some 16 km away. The signals were distributed by means of fiber-optic cables using a common fiber bundle between SPC 10 and the Apollo Complex, where the cables for each antenna were separated out. Ground system phase drifts were measured and removed in real-time, according to the procedures described in [4].

a) Lunar Doppler-delay imaging with the Radio Science Receiver (RSR):

The three antennas of the Apollo complex, DSS-24/25/26, are several hundred meters apart, hence each antenna experiences a slightly different Doppler frequency due to Earth rotation as observed from a distant point in space. Therefore, different Doppler frequencies must be applied to each antenna by means of pre-computed frequency predicts to ensure that each carrier arrives at the Moon with the same frequency. The reflected signal components were collected by another 34-m Beam Waveguide (BWG) antenna at the Venus Station, designated DSS-13, some 10 km from the Apollo Complex. Additional Doppler compensation was applied to the transmitted signals to account for the receiver location, such that the received signal arrived at the receiver centered at precisely 7.17964 GHz. This frequency was selected because it is the nominal receive frequency of the SDST aboard the EPOXI spacecraft, which also participates in communications related Uplink Array experiments as described in [2]. Frequencies were compensated for the center of the crater Tycho, and for the Mercury and Venus sub-radar points, as described in [3].

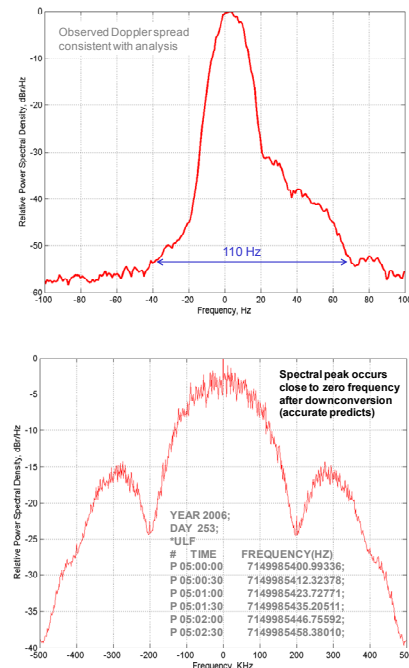


Figure 4. a) Doppler-broadened echo from the Tycho region; b) Spectrum of received PN-modulated echo.

Different Doppler slices on the Moon and planets impart different Doppler shifts to the signal as shown in Figs. 1, generating Doppler-broadened echoes, an example of which is shown in Fig. 4a where the target was the lunar crater Tycho. The main lobe of the scattered continuous wave (CW) signal spectrum from the Tycho region is seen to be approximately 50 Hz (about 40 dB below the peak), but spectral components out to 100 Hz and more also can be discerned 60 dB below the peak. Since the maximum Doppler broadening that can be generated by the lunar disk is approximately 140 Hz, these results are consistent with the expected spectral signature of an illumination pattern whose side lobes cover the entire lunar disk.

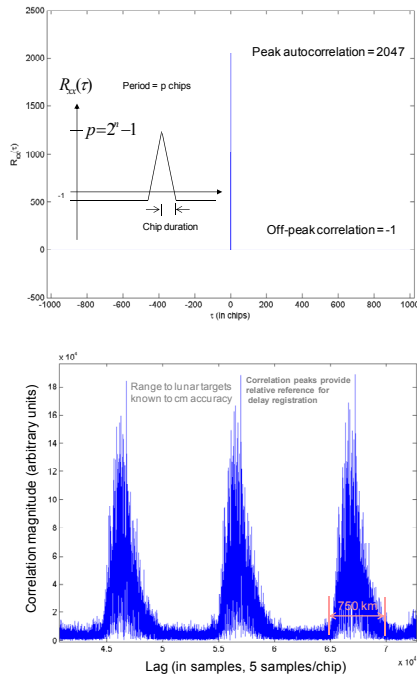


Figure 5. a) Theoretical and simulated autocorrelation function of PN11 sequence (2047 chips); b) Correlation property of experimentally observed echo from the Tycho region.

Whereas Doppler slices can be separated directly from the broadened echo even without modulating the signal, range resolution must be established by separating out delays scattered from different range rings. This operation is accomplished by modulating the carrier with a suitable PN sequence possessing good autocorrelation properties. With maximal-length PN sequences consisting of $M = 2^L - 1$ chips (or PN symbols), peak correlation proportional to M is achieved when the relative delay between the received signal and the local replica of the PN sequence is zero. For any other delay (measured in increments of chips), the circular autocorrelation is -1 , a factor of M smaller in magnitude than the peak of the correlation function, as shown in Fig. 5a. In order to match to the projected dimensions of a kilometer-sized pixel near the location of Tycho, range resolution of 750 m was selected by using a maximal-length binary PN sequence of $5 \mu\text{s}$ chip duration,

consisting of 2047 chips, modulated directly onto the carrier in a binary phase-shift-keyed (BPSK) format at 200 kHz chip-rate, resulting in the return spectrum shown in Fig. 4b. The return signal contained contributions from every illuminated range increment simultaneously. Signal components with different delays were separated out by correlating with a local replica of the transmitted PN sequence; an example of the correlation signature of the Tycho region is shown in Fig. 5(b) as a function of delay samples, corresponding to five samples per chip. Note that the same PN sequence is repeated continuously during transmission, resulting in a periodic correlation signature at the receiver.

The Doppler-delay images of Figs. 6 were processed with and without range compensation, to demonstrate the effect of range-smearing as the distance to the target changes during data-collection. The Doppler-delay imaging software developed earlier was modified to incorporate predict-based time-alignment, applied at the beginning of each PN sequence by adding in or skipping a sample as needed to keep up with the changing delay. This correction allowed for much longer integration times, and resulted in much less range-smearing in the image. Examples of the improvement through range-compensation is shown in Fig. 6: the image in Fig. 6a was obtained with 40-second integration but without range compensation, showing so much smearing that the crater Tycho and its surroundings can hardly be recognized. By contrast, the much longer 90-second range-compensated image of Fig. 6b, taken during the same track shows no evidence of smearing, easily resolving the crater walls and even showing some structure within the central peak.

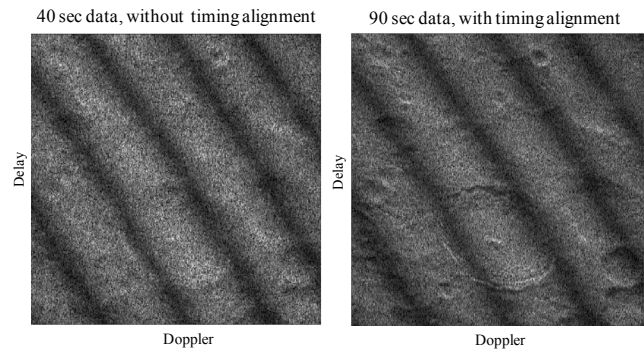


Figure 6. Comparison of Doppler-delay images of the lunar crater Tycho with and without range compensation, RSR receiver processing.

Since the primary purpose of demonstrating Uplink Array lunar/planetary capabilities is to provide high-EIRP illumination for distant targets, whereas in practice the processing of the received Doppler-broadened and delay-spread echoes will be carried out with the high-resolution Goldstone Solar System Radar (GSSR) receiver, it was decided to obtain simultaneous images with the GSSR receiver to compare with the RSR. This requires upconverting the 321.4 MHz intermediate frequency used by the RSR at DSS-13 to 460 MHz used by the GSSR, and

transmitting the IF signal via optical fiber to the GSSR receiver at DSS-14. Before describing and comparing the experimental images obtained from the RSR and GSSR receivers, a brief description of the GSSR receiver is provided.

b) GSSR Receiver Description

A copy of the received signal is routed to JPL's Goldstone Solar System Radar (GSSR) Receiver from the Uplink Array receiver located at DSS-13. The GSSR receiver first samples the data with an 8-bit ADC and records the digitized data in its disk array. GSSR software can simultaneously play back the data and perform delay compensation to remove time-drifting effects caused by the relative motions among the transmitter, target object, and the receiver. To compensate for these relative motions, we use ephemeris predictions expressed as 15-degree Chebychev polynomials to re-sample the received data. Such an ephemeris is also used to generate the Doppler predictions that will compensate for the Doppler shift experienced during transmission for the transmitting antenna. After the data are re-sampled, the Goldstone Solar System Radar (GSSR) software decodes the echo by cross-correlating the Doppler- and delay-compensated data with the expected PN sequence. This step is known as "range compression." Then an FFT is applied to appropriate pieces of the range-compressed data in order to generate Doppler-Delay images.

By performing these steps on a short segment of the data with a rough range delay prediction, an image can be obtained in near-real-time during the track for a quick check of echo detection. The highest resolution, but very time-consuming, data reduction can be performed after the track from the recorded data set.

c) Doppler-delay Imaging of the Planet Mercury, DSS-14 Illumination

Due to the proximity of the Moon, the radar echoes received at DSS-13 are strong enough to be observed with a room-temperature (effectively 100 kelvin) receiver, hence no attempt was made to install a cryogenic LNA for the initial Moon-Bounce Doppler-delay imaging experiments. As described in Section II, the lunar radar echoes are not thermally limited, but rather the dominant noise contribution is interference from PN-sequence modulated echoes arriving with non-integer delays, contributing the largest random components to the correlation output. With signal-interference-limited operation, increasing transmitter power does not improve target detectability, since the interference is proportional to the signal itself, and hence increases proportionally to the illuminating signal power.

However, as shown in Section II, radar echoes from Mercury and Venus are thermal-noise limited, hence reducing the receiver noise does improve the Doppler-delay

image, and enables successful observations with shorter integration times. Therefore, a cryogenic receiver was installed to receive planetary echoes, with a physical LNA temperature of approximately 15 kelvins, and effective system temperature at zenith of approximately 25 kelvins, providing 6 dB SNR gain over the room-temperature LNA. The lunar and planetary images in the following discussion were all obtained with the new cryogenic receiver at DSS-13.

In order to calibrate the cryogenic receiver and identify possible problems with the downconverter chains to the RSR and GSSR receivers, as well as optimize processing parameters for the best possible images, Mercury was first illuminated with the 70m antenna at DSS-14 transmitting 100 kW at 8.56 GHz on DOY-025 (January 25th), and received with the 8.56 GHz cryogenic LNA operating with 20 kelvin system temperature with the 34 meter antenna at DSS-13. First an unmodulated carrier was transmitted, Doppler-compensated to stop phase-rotation at DSS-13 (the receiving antenna). After a round-trip light-time of approximately 16 minutes on DOY-025, when Mercury was 0.975 AU from earth, a Doppler-broadened echo spanning roughly 300 Hz was observed on both the RSR and GSSR spectrum analyzers. Data was collected and post-processed to obtain the power spectral density (PSD) shown in Fig. 7, showing two low-frequency power-spikes within the Mercury echo that are believed to be downconversion artifacts. These were later eliminated by careful filtering for the DOY-121 Mercury track, which was a close encounter of Mercury and hence an ideal Uplink Array Doppler-delay imaging opportunity.

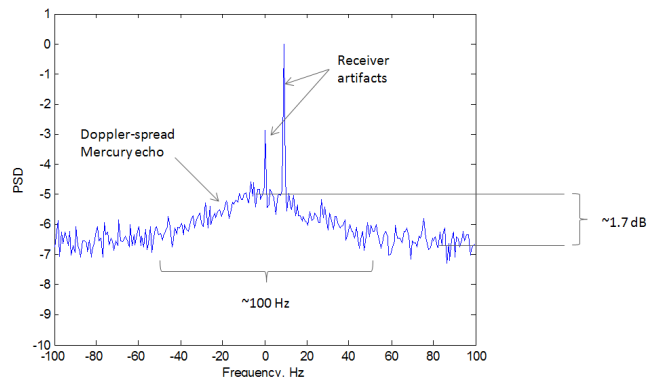


Figure 7. Doppler-spread CW echo of uplink-compensated X-band carrier, 8.56 GHz GSSR frequency, RSR processing.

Next, the carrier was phase-modulated with a PN sequence of length $2^{11} - 1 = 2047$, and the received signal composed of echoes with different range and Doppler analyzed via the RSR processing algorithms and with the GSSR receiver. The Doppler-delay image formed by the high-resolution GSSR receiver is shown in Fig. 8, showing a bright region at zero Doppler frequency due to reflections from the sub-radar point (center of image), and fainter upward-curving tails from the equator at increasing distance

from the sub-radar point, hence at greater range. Note that range increases upward in the GSSR image, hence features at greater range are mapped higher in the image than the equator. All detail from both the upper and lower hemispheres will be mapped above bright boundary defined by the equator, hence features from north and south will overlap in the image. However, with the faint images obtained on DOY-025, such overlapped features are not easily visible in Fig. 8.

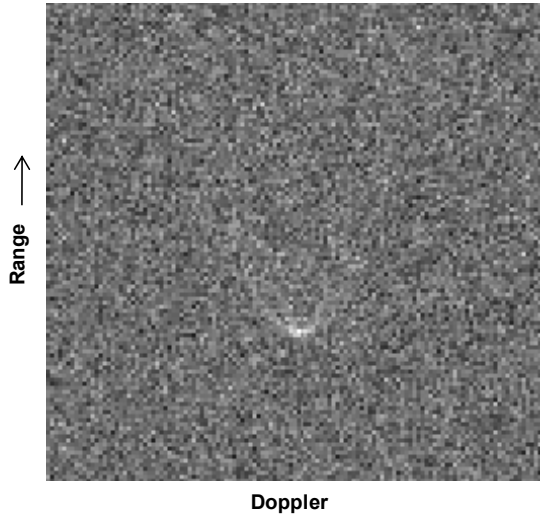


Figure 8. Doppler-delay image of Mercury obtained with the GSSR receiver on DOY-025, with 100 kW transmitter on the 70 meter antenna at DSS-14.

The echoes were also recorded with the RSR and processed according to the description in Section III, to obtain the images in Fig. 9. Note that in Fig. 9 increasing range is down, not up, because the RSR processing software was designed to image the crater Tycho located in the southern lunar hemisphere, where range increases downward on the lunar surface. This was not corrected on purpose, since it provides an easy way to distinguish between the RSR and GSSR images. The complex baseband samples collected by the RSR were at 1 MSPS rate, but had to be transferred to a different computer for processing, hence it took several minutes longer to obtain an image than with the GSSR receiver, where data-collection and Doppler-delay processing are performed on the same computer.

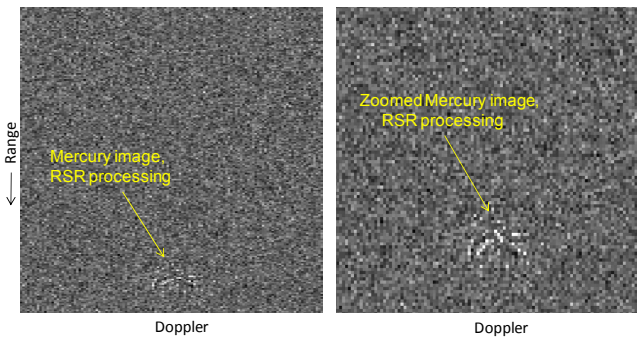


Figure 9. RSR processed images of the planet Mercury, obtained on DOY-025. 70 meter antenna at DSS-14 transmitting 100 kW at 8.56 GHz, 34 meter antenna at

DSS-13 receiving using 8.56 GHz cryogenic LNA.

The RSR processed image shown in Fig. 9 is clearly more pixelated than the GSSR image, which is attributed primarily to the sample-level range compensation used, where the PN-sequences are shifted by one sample when the range changes by $\tau=T/k$, where T is the chip-duration and k is the number of samples per chip. For our case, T is 5 microseconds, $k = 5$, hence τ is one microsecond. In the GSSR receiver, the range is applied continuously by resampling and interpolating, hence obtaining a smoother-looking image. We re-emphasize that the Uplink Array transmitter antennas were not involved in obtaining these images, only the Uplink Array signal processing equipment at DSS-13 was tested. Illumination was provided by the 70 meter antenna at DSS-14, transmitting 100 kW at 8.56 GHz, which was then received with an 8.56 GHz LNA receiver at DSS-13.

d) Doppler-delay Imaging of the Planet Mercury, DSS-24/25 Uplink Array Illumination

A Moon-Bounce experiment was conducted shortly before the Mercury encounter to refine the Uplink Array calibration phase, and to further compare RSR and GSSR processing characteristics. The Uplink Array was phased up, and images from the GSSR and RSR receivers obtained in near-real-time, shown in Fig. 10 a) and b). With 60 seconds of data and range compensation applied, the resolution of both receivers appears comparable, although the GSSR receiver image is somewhat smoother and brighter possibly due to the continuous interpolated range compensation applied by GSSR processing.

The apparent physical size of Mercury during the DOY-121 encounter is superimposed on the RSR Tycho image, demonstrating that Mercury will be much smaller than a DSS-24/25 fringe-width and hence the illumination will benefit from the full 6 dB array gain, if the two-element Uplink Array is properly phased up during this encounter. On the other hand, both southern and northern hemispheres will be illuminated simultaneously, causing north-south ambiguity and hence feature overlap in the Doppler-delay image.

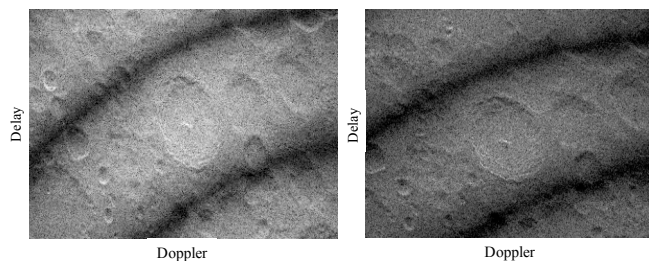


Figure 10. DSS-24/25 transmitting 25 kW, Uplink Array cryogenic receiver: a) GSSR and b) RSR processing, Tycho image comparison.

On May 1st, DOY-121, Mercury was illuminated with two of the three Apollo antennas DSS-24 and DSS-25, forming a two-element Uplink Array with a baseline of 258 meters. Both of these 34 meter antennas transmitted 20 kW of Doppler-compensated X-band at a nominal carrier frequency of 7.18 GHz, designed to stop phase-rotation at the DSS-13 receiver. The transmitters were calibrated, the frequency and pointing predicts uploaded, and measurements of ground-distribution round-trip phase and “cross-phase” recorded for both antennas. Both antennas were pointed at Mercury, and the previously recorded (DOY-109) calibration phase was applied to the DSS-24 phase-modulator. Note that with correct phasing, the EIRP generated by two 34 meter Uplink Array antennas is equivalent that of a 70 meter antenna, with the same transmitter power on each 34 meter as on the 70 meter antenna. However, since the 34 meter antennas could supply only 20 kW of power, the EIRP on DOY-121 was actually a factor of 5, or 7 dB, lower than during the DOY-025 track.

The cryogenic LNA front-end was operating at a physical temperature of 15 kelvins, yielding a system temperature of 27 kelvins at zenith. The X-band signal was downconverted to 321.4 MHz for the RSR receiver, and simultaneously to 460 MHz for the GSSR receiver (for this track, the GSSR receiver was transported to the DSS-13 control room, to facilitate comparison with RSR processing). To verify signal reception and array phasing, an unmodulated carrier was first transmitted from DSS-24 only (by shutting off the DSS-25 transmitter drive), and a Doppler-spread echo observed on the RSR spectrum analyzer after one RTLT = 16 minutes later. The signal was approximately 200 Hz wide, but only 0.4 dB above the noise-floor, so that real-time observation with short-duration FFT’s on the RSR was somewhat challenging, but a small signal was definitely noticeable. The averaged periodogram obtained from 12 minutes of data is shown in Fig. 11 a). Once the single-antenna signal was confirmed, the DSS-25 transmitter drive was enabled, and one RTLT later a much stronger signal, approximately 1.5 dB above the noise floor was observed. A simple calculation shows that this represents a factor of 3.75 increase, corresponding to 5.7 dB and close to the theoretically maximum 6 dB array gain, confirming that two-antenna Uplink Array phasing was accurate. Post-processed periodogram of 12 minutes of data is shown in Fig. 11 b). The carrier-echo was re-checked an hour later and still found to be 1.5 dB above the noise-floor, verifying that Uplink Array phasing continued to be accurate during the track.

Following verification of correct phasing, the 2047 PN-sequence modulation was initiated, and attempts were made to obtain a near-real-time image with the GSSR receiver. However, the gain was set too low initially, and an image could not be seen at first. The gain was increased and another attempt made about one hour later, resulting in a faint Mercury signature from the planet’s equator, as shown in Fig. 12 a). The FFT span used this time was smaller than

on DOY-025, hence the recorded arc-like Doppler-delay image is considerably larger, but exhibits the range-Doppler signature expected from a reflecting sphere with Lambertian scattering characteristics.

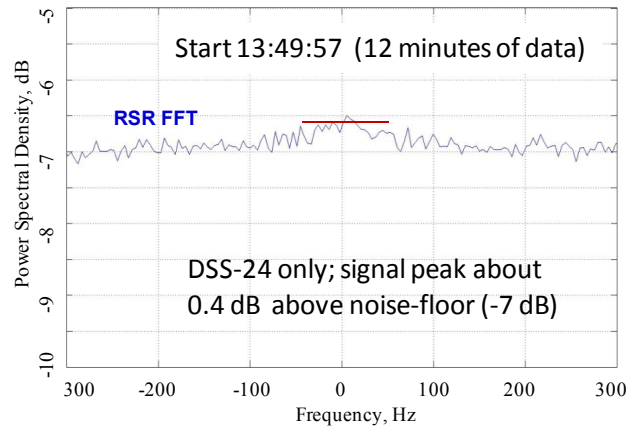


Figure 11a. a) Spectrum of echo power from Mercury, with a single 34 meter antenna transmitting 20 kW.

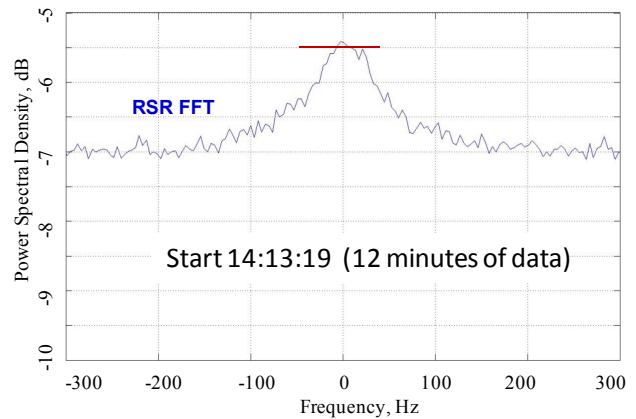
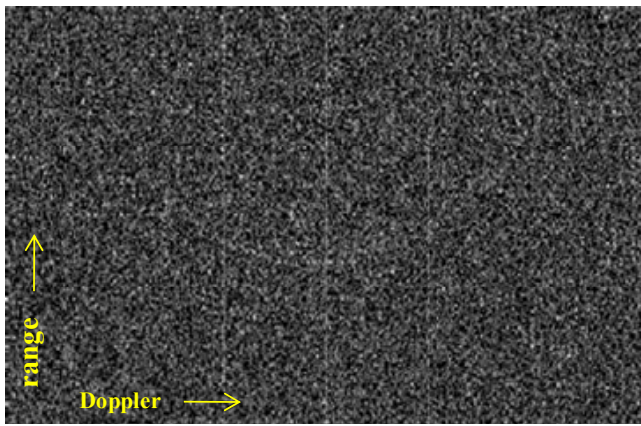


Figure 11. b) Two-antenna echo, demonstrating 6 dB increase in reflected signal power.

Post-processing of the recorded data failed to improve the initial near-real-time GSSR image significantly, and attempts to extract a Doppler-delay image from subsequent data-records (after 1600 UTC) yielded no additional images. It was hypothesized that the computer clock may have been off by one or more seconds in either direction, and the recorded data re-processed with timing delays of +/- 1 second inserted, resulting in the images of Fig. 12 b), which show minor deterioration on the right-hand-side of the sub-radar point for both time offsets. With larger offsets of several seconds the image washed out completely, suggesting that computer clock offset was not the cause of the unexpectedly faint image.



GSSR computer clock accuracy test

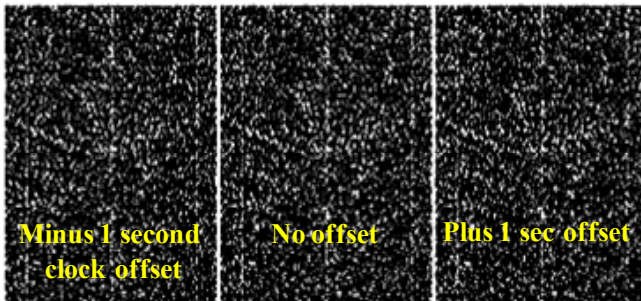


Figure 12. a, b. First faint Mercury Doppler-delay images obtained at the May 1st 2010 close encounter, with a two-element Uplink Array and 34 meter receiver.

e) Doppler-delay Imaging of the Planet Venus, with DSS-24/26 Uplink Array Illumination

A relatively short, two-hour long tracking opportunity with Venus visibility was scheduled on DOY-297, October 24th 2010, when Venus was only 0.275 AU from earth. The two Apollo antennas with the longest available Uplink Array baseline of 500 meters, DSS-24 and DSS-26, were scheduled for this track. However due to problems with the DSS-26 subreflector positioner, the DSS-25 antenna was exchanged for the DSS-26 antenna during this critical imaging track. Although the DSS-24/26 generates the narrowest possible Apollo array fringes in the far-field, almost a factor of 2 narrower than that of the DSS-24/25 baseline, the DSS-24/25 baseline nearly resolves Venus.

At the time of the Venus track, on DOY-297, Venus was only 0.275 AU from earth, resulting in an RTLT of 5 minutes, much shorter than the 16 minute RTLT from Mercury. As with the Mercury imaging track, an unmodulated X-band carrier of nominal 7.18 GHz was transmitted initially from DSS-25, and a strong echo observed on the RSR and GSSR FFT processors one RTLT (5 minutes) later. The DSS-24 driver was enabled, and a 6 dB stronger signal observed another RTLT later. Both

periodograms are shown in Fig. 13 from the GSSR receiver (arbitrary power units), and in Fig. 14 from the RSR receiver.

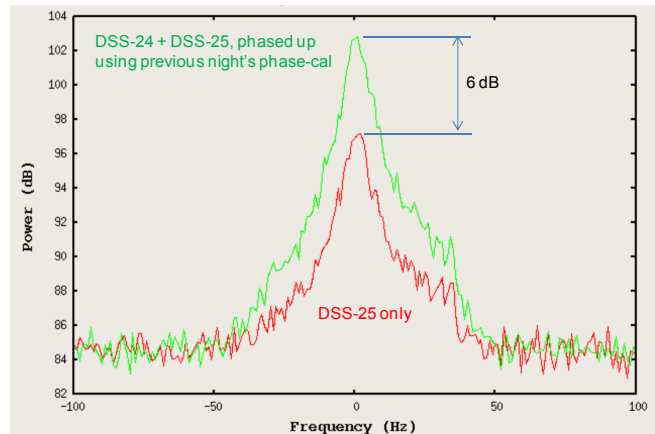


Figure 13. Venus echo for single antenna and two-antenna Uplink Array illumination with GSSR processing, demonstrating 6 dB array gain for the two-antenna array.

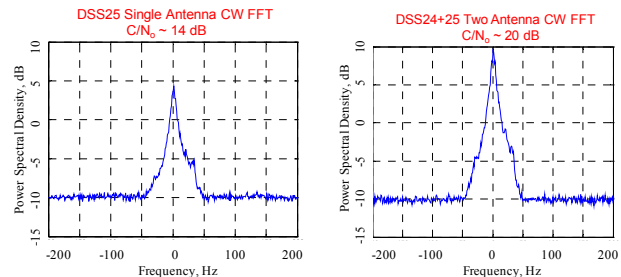


Figure 14. Venus echo for single antenna and two-antenna Uplink Array illumination with RSR processing, showing SNR's of 14 and 20 dB, respectively above the noise floor, demonstrating 6 dB array gain for the two-antenna array.

Note that in Fig. 14a the single-antenna echo is 14 dB above the noise-floor, in good agreement with the analytical prediction of 14.9 dB in Section II, whereas the coherently added two-antenna echowas 20 dB above the noise-floor, as shown in Fig. 14b. This was sufficient confirmation of correct array phasing, hence the PN-modulation was enabled in preparation for Doppler-delay imaging.

Venus has a delay-depth of 40 msec, but also a dense CO₂-rich atmosphere that attenuates the radar signal by approximately 10 dB at zenith, hence it was assumed that only the region near the sub-radar point would reflect significant signal energy, therefore the chip-duration was not altered from the lunar imaging scenario of 5 microseconds duration and the same 2047 PN11 sequence was used. Phase-modulated Uplink Array signal transmission commenced at about 1900 UTC, resulting in the Doppler-delay images from the GSSR receiver shown in Fig. 15a. Since the highest-EIRP illumination from the

phased Uplink Array occurs at the equator, there is north-south ambiguity present, resulting in superimposed images of Venusian features from above and below the equator.

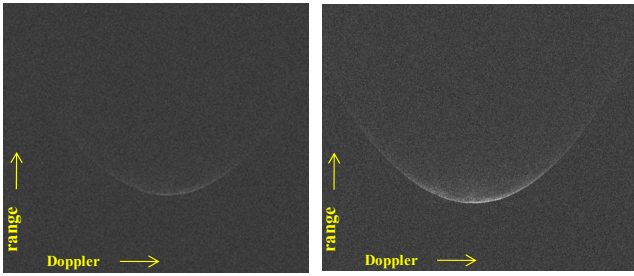


Figure 15. Doppler-delay images of Venus, taken on DOY-297, GSSR processing: a) single antenna illumination (DSS-25); b) two-antenna phased-array illumination (DSS-24 + DSS-25), showing greatly improved image quality. Range increases along the vertical axis, Doppler is along the horizontal axis.

Next, the DSS-25 transmitter was enabled, generating much brighter and detailed image, shown in Fig. 15b. The corresponding images from the RSR receiver are shown in Figs. 16, where now the range increases downward in order to generate visually correct Doppler-delay images near the crater Tycho, which is used for Uplink Array calibration as explained in [1, 2]. Since Tycho is located in the lunar southern hemisphere, range was set to increase in the downward direction with RSR processing. The total Doppler range displayed is about 10 Hz for the GSSR and 25 Hz for RSR processing, centered around the sub-radar point in these images.

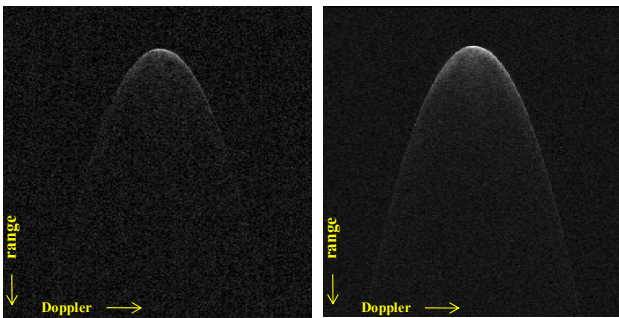


Figure 16. Doppler-delay images of Venus, taken on DOY-297, RSR processing: a) single antenna illumination (DSS-25); b) two-antenna phased-array illumination (DSS-24 + DSS-25), showing greatly improved image quality. Range decreases along the vertical axis, Doppler is along the horizontal axis.

The relatively long baseline of the DSS-24/25 array creates relatively narrow fringes in the far-field capable of almost resolving Venus perpendicular to the baseline, and since the baseline is roughly perpendicular to the Venusian equator during transit (the time of this track), it is possible to move

the brightest part of the principal fringe above and below the equator by applying +/- 90 degree phase-shifts to the DSS-24 phase modulator. This approach was indeed tried, resulting in the two GSSR images shown in Fig. 17, and the corresponding RSR images shown in Fig. 18. For both cases, the region above the equator is imaged in a), and the region below the equator in b). The fact that the two images are not of equal intensity implies that a small negative phase offset was present when the images were taken, moving the fringes further down from the equator than intended, hence receiving a weaker echo due to greater slant illumination and greater atmospheric absorption.

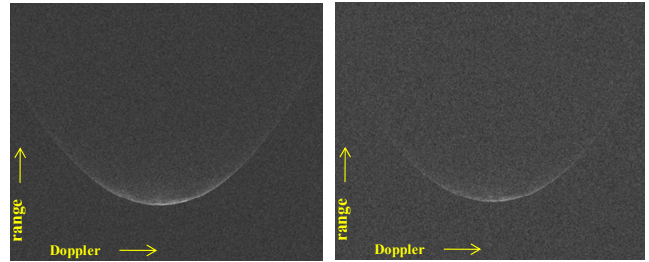


Figure 17. Attempted resolution of north-south ambiguity, GSSR processing: a) +90 degree phase applied, northern hemisphere, b) -90 degree phase applied, southern hemisphere. Range increases along the vertical axis, Doppler is along the horizontal axis.

In both sets of images, somewhat different features can be discerned near the equator along the sub-radar point, but longer integration and more refined processing will be required to clearly identify features with any certainty. The results of more sophisticated processing of this data will be the subject of a future paper.

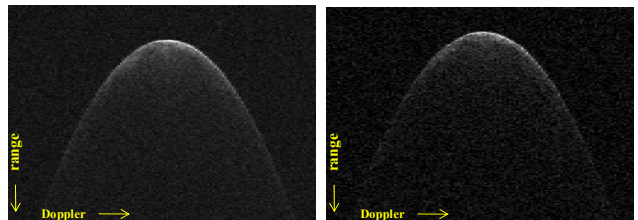


Figure 18. Attempted resolution of north-south ambiguity, RSR processing: a) +90 degree phase applied, northern hemisphere, b) -90 degree phase applied, southern hemisphere. Range decreases along the vertical axis, Doppler is along the horizontal axis.

This idea was intended to demonstrate a key advantage of two-element Uplink Arrays configured to illuminate planetary radar targets, namely that by increasing the baseline the array can potentially resolve the north-south ambiguity plaguing conventional single-antenna illumination, even with the largest terrestrial apertures such as the Arecibo antenna. By placing the baseline of two Uplink Array antennas in the terrestrial north-south

direction, resolution of the terrestrial planets Mercury, Venus and Mars becomes feasible provided the baseline is commensurate with the angular resolution required for the target planet. Future experiments will employ the longer DSS-24/26 baseline, which generates narrower fringes and hence resolves the northern and southern hemispheres of nearby planets such as Venus and Mars at close encounters.

5. SUMMARY AND CONCLUSIONS

The application of the DSN's 34 meter antennas configured as an Uplink Array to lunar and planetary imaging has been described and analyzed. Although initially developed to calibrate the Uplink Array, Moon-Bounce Doppler-delay imaging capabilities have now been applied to planetary radar applications by providing high-EIRP, high-resolution illumination for nearby solar system targets such as Mercury and Venus, and in the future Mars and near-earth asteroids as well. The concept of Doppler-delay imaging has been described and analyzed, supported by experimental evidence obtained from lunar and planetary radar imaging experiments. It was shown that lunar imaging quality depends on the ability to average signal-dependent interference that cannot be improved by longer integration, whereas planetary imaging is dominated by thermal noise where longer integration has a direct impact on imaging quality. Results for lunar and planetary imaging of Mercury and Venus have been presented, proving that Uplink Arrays can provide sufficient EIRP to enable continuation of solar system radar even if the large 70 meter antenna at DSS-14 is not available for planetary radar imaging applications.

Acknowledgment: The research was carried out at the Jet Propulsion Laboratory, California Institute of Technology, under a contract with the National Aeronautics and Space Administration.

REFERENCES

- [1] V. Vilnrotter, R. Mukai, and D. Lee, "Uplink Array Calibration via Far-Field Power Measurement," *The Interplanetary Network Progress Report*, vol. 42-164, Jet Propulsion Laboratory, Pasadena, California, pp. 1–16, February 15, 2006.
- [2] V. Vilnrotter, D. Lee, R. Mukai, T. Cornish, P. Tsao, "Three-Antenna Doppler-Delay Imaging of the Crater Tycho for Uplink Array Calibration Applications," IPN Progress Report 42-169, Jet Propulsion Laboratory, May 15, 2007.
- [3] J.-L. Margot, D. Campbell, R. Jurgens, M. Slade, "Digital Elevation Models of the Moon from Earth-Based Radar Interferometry," *IEEE Transactions on Geo-Science and Remote Sensing*, Vol. 38, No. 2, pp. 1122-1133, March 2000.

[4] P. Tsao, V. Vilnrotter, V. Jamnejad, "Pointing-Vector and Velocity Based Frequency Predicts for Deep-Space Uplink Array Applications," IEEE Aerospace Conference Proceedings, Big Sky, Montana, March 2009.

[5] L. Paal, R. Mukai, V. Vilnrotter, T. Cornish, D. Lee, "Ground System Phase Estimation Techniques for Uplink Array Applications," IPN Progress Report 42-167, Jet Propulsion Laboratory, November 15, 2006.

[6] V. Vilnrotter, D. Lee, T. Cornish, P. Tsao, L. Paal, V. Jamnejad, "Uplink Array Concept Demonstration with the EPOXI Spacecraft," IEEE Aerospace Conference Proceedings, Big Sky, Montana, March 2009.

[7] *Multyear Interactive Computer Almanac*, US Naval Observatory, Willmann-Bell, 2005. ISBN 0-943396-84-0

[8] Seidelmann, P. *Explanatory Supplement to the Astronomical Almanac*, University Science Books, 1992. pp. 127-130.

[9] Shapiro, I. "Fourth Test of General Relativity" *Phys Review Letters* 13, 1964, pp. 789-791.

[10] T. D. Moyer, "Formulation for Observed and Computed Values of Deep Space Network Data Types for Navigation," Jan. 2003, Wiley-Interscience, 576 pp. ISBN-13: 978-0471445357.

BIOGRAPHY



Victor Vilnrotter (M'79, SM'02) received his Ph.D. in electrical engineering and communications theory from the University of Southern California in 1978. He joined the Jet Propulsion Laboratory, Pasadena, Calif., in 1979, where he is a Principal Engineer in the Communication Architectures and Research Section.

His research interests include electronic compensation of large antennas with focal-plane arrays, adaptive combining algorithms for large antenna arrays, optical communications through atmospheric turbulence, the application of quantum communications to deep-space optical links, and the development of uplink array calibration and tracking technologies. He has published extensively in conferences and refereed journals, and has received numerous NASA awards for technical innovations.



Dennis K. Lee (S'97 M'98) earned his B.S. from Case Western Reserve University in 1997 and his M.S. from Rensselaer Polytechnic Institute in 1998, both in Electrical Engineering. Since 1999, he has been a member of technical

staff in the Digital Signal Processing Research group at the Jet Propulsion Laboratory. Currently, his research interests include bandwidth efficient modulations and high rate signal processing.



Philip Tsao is a member of the Communications Networks Group at JPL. He received a BEE from Georgia Tech in 1999 and an MSEE from Caltech in 2001 where he pursued research in collective robotics. From 2001 and 2005 he was a Systems Engineer with Raytheon Space and Airborne Systems where he supported radar software and mixed signal circuit design efforts.



Timothy Cornish received a B.S. degree in Electrical Engineering from Illinois Institute of Technology in 1995. He has been employed in private industry in the high power transmitter field for over 15 years in positions ranging from Design Engineer to Engineering Department Manager. During that time he was responsible for system engineering and project management in the development of the 4 kW X-band High Power Amplifier recently in use in the Deep Space Network 34m Beam Waveguide Stations. Timothy joined the Jet Propulsion Laboratory in 2000 as a Transmitter Design Engineer in the Communications Ground Systems Section and is currently System Engineer for the Deep Space Network Uplink Subsystem. In his position as Transmitter Design Engineer he was responsible for the design of the 20 kW X-Band High Power Amplifier currently in use in the Deep Space Network 34m Beam Waveguide Stations.